A molecular dynamics study on oxidation of aluminum hydride (AlH_3)/hydroxyl-terminated polybutadiene (HTPB) solid fuel

Muye Feng[a], Heping Li[b,c], Kai H. Luo[b,*]

[a] *Center for Combustion Energy, Key Laboratory for Thermal Science and Power Engineering of Ministry of Education, Department of Energy and Power Engineering, Tsinghua University, Beijing 100084, China*

[b] *Department of Mechanical Engineering, University College London, Torrington Place, London WC1E 7JE, UK*

[c] *School of Science, Hangzhou Dianzi University, Hangzhou 310018, China*

Abstract

Aluminum hydride (AlH_3) is a promising replacement for aluminum in hybrid and solid propellants, where hydroxyl-terminated polybutadiene (HTPB) is normally used as a binder. In this study, a reactive molecular dynamics simulation method is employed to investigate the fundamental oxidation mechanisms of AlH_3/HTPB solid fuel using a core-shell nanoparticle configuration. The overall oxidation is found to proceed in three distinctive stages: (I) preheating, (II) acceleration and (III) oxidation. Furthermore, oxidation mechanisms of AlH_3 and HTPB are separately studied to understand their different roles during the overall oxidation process. With respect to the oxidation of the AlH_3 nanoparticle, the reaction is delayed compared with the oxidation of pure AlH_3, due to the initial coverage of the nanoparticle surface by HTPB molecules. Additionally, decomposition of HTPB/HTPB intermediates is observed to occur on the nanoparticle surface and some of the decomposed products are integrated with the nanoparticle. In the meantime, the AlH_3 nanoparticle facilitates the HTPB initiation by dehydroxylation or dehydrogenation. Moreover, the primary decomposition pathway of HTPB/HTPB intermediates is the continuous scission of carbon chain to form a large amount of C_4 species, which are finally oxidized at a later stage of the reaction producing

* *Corresponding author at: Department of Mechanical Engineering, University College London, Torrington Place, London WC1E 7JE, UK. Tel: +44 (0)20 7679 3916. E-mail address: k.luo@ucl.ac.uk (Kai H. Luo)*

CO, CO_2 and H_2O. The new atomistic insights obtained from the present research could potentially benefit the design of AlH_3/HTPB-based solid propellants.

Keywords: AlH_3/HTPB solid fuel; Oxidation; Molecular dynamics; Reactive force field

1. Introduction

Aluminum hydride (AlH_3) is a promising ingredient used in a wide range of propulsion systems [1, 2], which has been extensively studied in the past decades [3-6]. AlH_3 has a high gravimetric (10.1 wt %) and volumetric (149 kg/m^3) hydrogen capacity [7] and has been recognized as an excellent replacement for aluminum in hybrid and solid propellants [8]. Replacing Al with AlH_3 can result in more than 10% increase in specific impulse over currently used rocket propellants [9]. Additionally, the flame temperature and average molecular mass of the combustion products can be reduced in the presence of AlH_3 [8]. Despite these advantages, the practical use of AlH_3 in propellants suffers from some issues including strong sensitivity to oxidation and hydration, and low thermal stability [10]. Hydroxyl-terminated polybutadiene (HTPB) is an oligomer of butadiene terminated with a hydroxyl group at each end, which is a standard binder formulated in Al or AlH_3-based solid propellants [8, 11]. The nature and composition of HTPB make it also a fuel that is involved in the combustion process. Therefore, understanding of the oxidation of AlH_3/HTPB composite is of great theoretical and practical importance.

However, compared with pure AlH_3, the decomposition and oxidation of AlH_3/HTPB composite system are rarely investigated. Among the few previous studies, Young et al. [12] compared the combustion characteristics of Al/HTPB and AlH_3/HTPB solid fuels using nitrous oxide as the oxidizer and found that the regression rate of HTPB was increased by approximately 20% with a 40 wt % AlH_3 loading, whereas the addition of Al at all loadings (10-40%) decreased the regression rate of HTPB. Chen et al. [13] also observed the improvement (up to 57.2%) in the HTPB regression rate with AlH_3 and attributed it to the rapid H_2 release from AlH_3 dehydrogenation forming a porous layer. While these studies have revealed the enhancement of HTPB combustion with the addition of AlH_3, detailed

understanding of the whole oxidation process is lacking. In this study, reactive molecular dynamics (MD) simulations are employed to investigate the fundamental oxidation mechanisms of AlH_3/HTPB solid fuel. In addition, the oxidation mechanisms of AlH_3 and HTPB are also separately scrutinized to gain deeper insights into their different roles and mutual interactions during the overall oxidation process.

2. Methods

2.1. ReaxFF molecular dynamics

The reactive force-field molecular dynamics (ReaxFF MD) combines the advantages of quantum mechanics (QM) and the classic MD to form a powerful yet computationally affordable simulation approach for reactive systems. It undercuts the prohibitive computational cost of QM while overcoming the inability of the classic MD for simulating chemical reactions [14, 15]. The ReaxFF MD is therefore an efficient method to study the long-time large-scale reactive systems that are impractical or impossible for either QM or classic MD methods. The ReaxFF is based on the bond-order concept and the force field parameters are trained with QM calculations or/and experimental data to give it accuracy and fidelity. To describe the dissociation, transition and formation of chemical bonds, ReaxFF bond orders are calculated directly from interatomic distances as shown in Eq. (1) [15]:

$$\begin{aligned} \mathrm{BO}_{ij} &= \mathrm{BO}_{ij}^{\sigma} + \mathrm{BO}_{ij}^{\pi} + \mathrm{BO}_{ij}^{\pi\pi} \\ &= \exp\left[p_{\mathrm{bo1}} \left(r_{ij} / r_o^{\sigma} \right)^{p_{\mathrm{bo2}}} \right] + \exp\left[p_{\mathrm{bo3}} \left(r_{ij} / r_o^{\pi} \right)^{p_{\mathrm{bo4}}} \right] + \exp\left[p_{\mathrm{bo5}} \left(r_{ij} / r_o^{\pi\pi} \right)^{p_{\mathrm{bo6}}} \right] \end{aligned} \tag{1}$$

where BO is the bond order between atoms *i* and *j*, r_{ij} is interatomic distance, r_o terms are equilibrium bond lengths, and p_{bo} terms are empirical parameters. The general expression of the ReaxFF potential consisting of different energy contributions is given in Eq. (2) [16]:

$$E_{\mathrm{system}} = E_{\mathrm{bond}} + E_{\mathrm{over}} + E_{\mathrm{under}} + E_{\mathrm{lp}} + E_{\mathrm{val}} + E_{\mathrm{tor}} + E_{\mathrm{vdWaals}} + E_{\mathrm{Coulomb}} \tag{2}$$

where E_{system}, E_{bond}, E_{over}, E_{under}, E_{lp}, E_{val}, E_{tor}, $E_{vdWaals}$ and $E_{Coulomb}$ represent total energy, bond energy, overcoordination energy penalty, undercoordination stability, lone pair energy, valence angle energy, torsion angle energy, van der Waals energy and Coulomb energy, respectively.

The ReaxFF MD methodology has been successfully applied in a broad range of reactive systems [17-21]. Detailed information on ReaxFF including its development and exhaustive formulation can be found in references [15, 16].

2.2. Simulation details

The parameter set for Al/C/H/O interactions [22], which was extended from the original Al/H description [23] specifically parameterized for aluminium hydride is chosen as the force field used in this study. The original Al/H force field is capable of describing the reaction of AlH_3 clusters and their dehydrogenation process. After the upgrade from Al/H to Al/C/H/O, the force field incorporates hydrocarbons as well as oxidation reactions thereby allowing the investigation of mutual interaction between Al- and hydrocarbon-based materials during the oxidation process. Hence, this Al/C/H/O force field covers all of the chemical reactions that may occur in the research. The present simulations consist of two main parts: (1) system construction and equilibration under the canonical (NVT) and isothermal-isobaric (NPT) ensembles, and (2) oxidation reaction under the microcanonical (NVE) ensemble. Three independent runs are conducted for the final oxidation system, and the results are averaged for analysis. Error bars (color filling around the curve) shown in the present study are determined by the standard error of the mean. The time step used is 0.2 fs and the simulation data are outputted at an interval of 0.2 ps. A commonly used 0.3 bond order cutoff is employed to analyse the species formed. All of the ReaxFF MD simulations are performed using the LAMMPS package [24] and the visualization of simulation data is conducted through OVITO [25].

2.3. System construction

In order to approximate the realistic experimental condition, the following procedure for system construction is carried out:

Due to the existence of an oxide layer on AlH_3, the core-shell AlH_3/Al_2O_3 structure is first built following these steps: (1a) cut a 5 nm diameter α-AlH_3 nanoparticle from the crystal structure and relax it for 100 ps; (1b) cut the 3.5 nm diameter core from the relaxed AlH_3 nanoparticle; (2a) cut a 6 nm diameter α-Al_2O_3 nanoparticle from the crystal structure and relax it for 100 ps; (2b) create the amorphous Al_2O_3 by annealing [26] the relaxed Al_2O_3 nanoparticle for 100 ps (experimental results reported that the surface oxide layer covering the AlH_3 is amorphous Al_2O_3 [27]); (2c) cut a 0.5 nm thickness shell from the annealed Al_2O_3 nanoparticle (radius from 1.75 to 2.25 nm); (3) combine the AlH_3 core and Al_2O_3 shell together and then relax the core-shell structure for 100 ps. The core-shell nanoparticle contains 5670 atoms (801 core Al, 954 shell Al, 2525 H, and 1390 shell O atoms, respectively). After the relaxation, a small amount of core H atoms have diffused into the oxide shell and to the nanoparticle surface as seen in Fig. 1a. All of the relaxation processes are performed at 300 K and the temperature during annealing is heated up to 2500 K under the NVT ensemble.

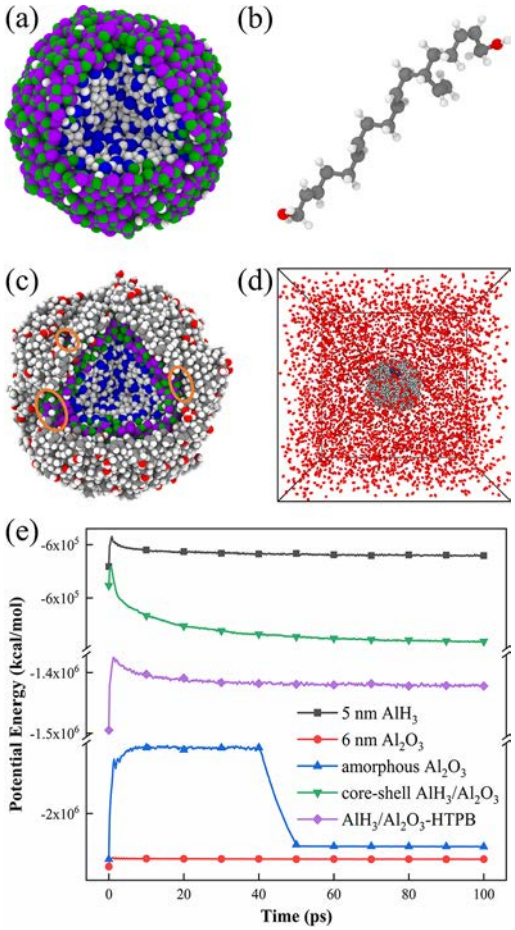

Fig. 1. Illustration of key stages and potential energy profiles of relaxation and equilibration processes during the system construction: (a) relaxed core-shell AlH_3/Al_2O_3 structure; (b) energy minimized HTPB molecule; (c) equilibrated AlH_3/Al_2O_3-HTPB composite (orange circles show the typical nanoparticle exposed areas); (d) oxidation simulation system; (e) potential energy profiles of relaxation and equilibration processes. Atoms colouring scheme: core Al - blue; shell Al - purple; H - white; shell O - green; HTPB & molecular oxygen O - red; C - grey.

Next, the HTPB model is constructed. HTPB contains different butadiene isomers, including a: cis-1,3-butadiene, b: vinyl-1,2-butadiene, and c: trans-1,3-butadiene. The proportion of a, b and c components of HTPB is about 1:1:3 [28], so a simplified HTPB molecule ($C_{20}H_{32}O_2$) comprising one cis-, one vinyl-, and three trans-form butadiene units terminated with a hydroxyl group at each end is adopted. Energy minimization is performed on the HTPB molecule to obtain an optimized structure (Fig. 1b).

The formulation of AlH_3/HTPB-based solid propellant varies [8, 11] and a generic mass fraction ratio of 5:3 for the AlH_3/Al_2O_3 nanoparticle and HTPB is used in the present study, resulting in 142 HTPB molecules. These HTPB molecules are initially placed around the core-shell nanoparticle, followed by the NPT equilibration at 300 K and 15 atm for 100 ps to simulate the physical process of preparing the AlH_3/Al_2O_3-HTPB composite. After the equilibration, some core-shell nanoparticle exposed areas with random shape and size can be seen on the composite surface (Fig. 1c), which is reasonable as HTPB acts as the binder rather than the coating material for AlH_3 in the solid propellant.

Finally, the prepared AlH_3/Al_2O_3-HTPB composite model is positioned at the centre of a 200 Å × 200 Å × 200 Å periodic simulation box filled with 5100 oxygen molecules (Fig. 1d), the number of which is enough for complete oxidation. This simulation system constructed for oxidation reaction contains 23538 atoms in total and starts from 300 K under NVE ensemble.

Every simulation system undergoes energy minimization before running to eliminate artificial effects from the initial geometric configuration. The potential energy profiles during the system construction are given in Fig. 1e, proving that 100 ps is enough for all of the relaxation and equilibration processes.

3. Results and discussion

3.1. Overall oxidation process

The oxidation reaction is found to proceed in three main stages, which can be characterised by the time evolution of temperature and the number of key species as shown in Fig. 2. The temperature of the whole system, the AlH_3/Al_2O_3 core-shell nanoparticle and the rest excluding the nanoparticle are all monitored. Any atom leaving the nanoparticle is excluded in the calculation of the nanoparticle temperature.

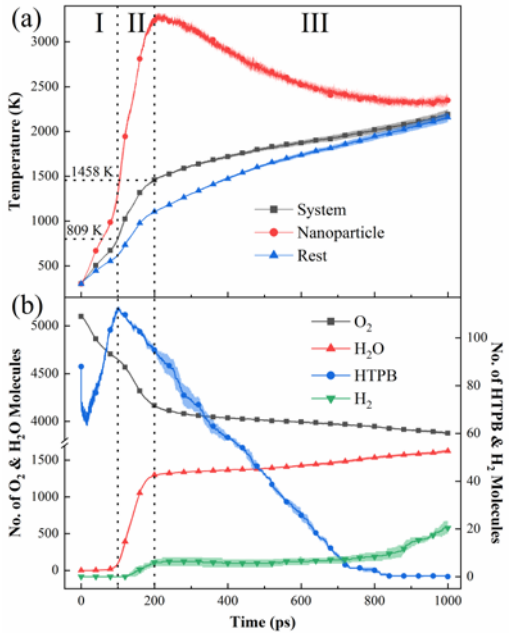

Fig. 2. Three main stages for the oxidation reaction characterised by the time evolution of (a) temperature and (b) number of key species. Stage I (0-100 ps): preheating; Stage II (100-200 ps): acceleration; Stage III (200 ps onward): moderate oxidation.

At Stage I from 0 to 100 ps, all of the three temperatures rise and the temperature of the nanoparticle climbs faster than that of the rest (1313 and 625 K at 100 ps, respectively), with a system temperature of 809 K at the end of Stage I. The sublimation of HTPB around the nanoparticle is observed, which leads to the increase in its molecule number. An initial shape decrease of HTPB number is noticed because the expansion of the HTPB layer is faster inside than outside leading to the instantaneous proximity between HTPB molecules at the beginning. During the sublimation, the outside HTPB molecules are released directly, whereas those inside ones on the nanoparticle surface first have O of OH from one end adhering on the surface Al atoms with the carbon chain freely hanging in the air (Fig. 3d), and then leave the surface gradually. This demonstrates that the terminal OH groups of HTPB are important for binding. Some HTPB molecules lose their terminal H or OH when departing from the nanoparticle surface, which are integrated with the nanoparticle eventually. Figure 3 illustrates the HTPB sublimation process during Stage I. At 100 ps, less than 10 HTPB molecules stay on the nanoparticle surface. As HTPB sublimates, the exposed surface areas of the nanoparticle

become increasingly large and adsorb ambient O_2 molecules. At the end of this stage, only H_2O starts to appear and no significant product formation is observed. To summarize, Stage I can be designated as the preheating stage accompanied by system temperature rise, HTPB sublimation and O_2 adsorption on the nanoparticle.

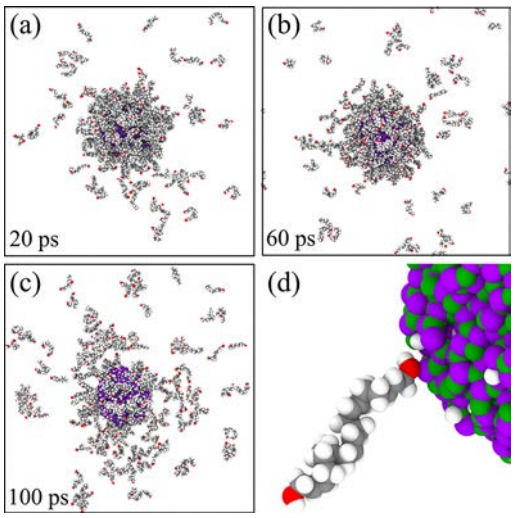

Fig. 3. Process of HTPB sublimation during Stage I of the oxidation reaction: (a) t = 20 ps; (b) t = 60 ps; (c) t = 100 ps; (d) an example of O of OH from one end of HTPB adhering on the nanoparticle surface Al atom with the carbon chain freely hanging in the air. Only the nanoparticle and HTPB molecules are shown for a clear visualization.

Stage II starts from 100 to 200 ps, where a significant change in both temperature and the number of key species occurs. Although the climbing rate of the three temperatures is all faster than those at Stage I, the temperature of the nanoparticle remarkably increases to about 3300 K compared with the relatively smooth temperature growth of the rest and the system to 1105 and 1458 K, respectively at the end of Stage II. This suggests that the nanoparticle reaction dominates the overall oxidation at Stage II. While there are still a few HTPB molecules remaining on the nanoparticle at the end of Stage I, the total number of HTPB begins to drop from its peak point owing to the initiation of HTPB. In the meantime, the rapid consumption of O_2 continues, which participates in the reaction of both nanoparticle and HTPB. Significant H_2O production mainly from the nanoparticle is detected and the formation of H_2 emerges with a delay at about 120 ps. The mechanisms and product generation of the

nanoparticle and HTPB reactions are analysed in detail in the following sections. Stage II can be identified as the acceleration stage with considerable temperature rise and product release, the duration of which is almost the same as the preheating stage. The system temperature at the beginning of Stage II is 809 K, which agrees well with Chen et al.'s [13] experimental results that the burning temperature of AlH_3/HTPB solid fuels is around 800 K leading to the ignition and combustion.

From 200 ps onward, the reaction enters into stage III: oxidation. The system temperature increases steadily from 1458 to about 2200 K at the end of the simulation. During this stage, the nanoparticle temperature gradually falls from its maximum and tends to be stable in the end but the temperature of the rest still goes up and approaches the system temperature. This indicates that the HTPB reaction plays a dominant role at Stage III. Consistently, the number of HTPB molecules keeps decreasing at a similar speed as in Stage II. Meanwhile, the reduction in O_2 and growth in H_2O populations are both smooth because of the dominant HTPB and stabilized nanoparticle oxidation. A second noticeable increase in H_2 production starts after about 700 ps when the HTPB consumption nearly completes, which results from the reaction of HTPB intermediates.

3.2. Mechanisms of AlH_3/Al_2O_3 core-shell nanoparticle oxidation

The reaction mechanisms of the nanoparticle during the overall oxidation process are investigated. Figure 4 depicts the evolution of structure and composition of the nanoparticle. Initially at 0 ps, in addition to the diffusion of a small number of core H atoms into the shell and to the surface, terminal OH groups of HTPB are adsorbed on the surface Al atoms. At 50 ps, as HTPB sublimates, ambient O_2 molecules are adsorbed on the nanoparticle surface and more core H atoms diffuse outward with the shrinking of the core-shell boundary but there is no product formation. Coming to 100 ps, the amount of core H atoms is apparently reduced and the core-shell boundary is further contracted. Simultaneously, the O-O bond of ambient O_2 is broken and these free O atoms penetrate into the nanoparticle. This is also the time when the significant product release starts at Stage II. Until 150 ps, most of the core H atoms are released with the core area complemented by shell O atoms. At 200 ps,

only a few H atoms can be seen in the nanoparticle and the ambient O atoms advance deeper into the nanoparticle. From 200 ps to the end (Stage III), the core/shell Al atoms are mixed with each other. In the meantime, the ambient O atoms continuously flow into the nanoparticle. According to Fig. 2b, the production of H_2O is prior to and much more significant than that of H_2, which is attributed to the small size and high specific surface area of the nanoparticle. It is noteworthy that C atoms (maximum number less than 200 within the 1000 ps simulation) are found on the nanoparticle surface as the HTPB/HTPB intermediates could decompose on the surface and some of the decomposed products are integrated with the nanoparticle.

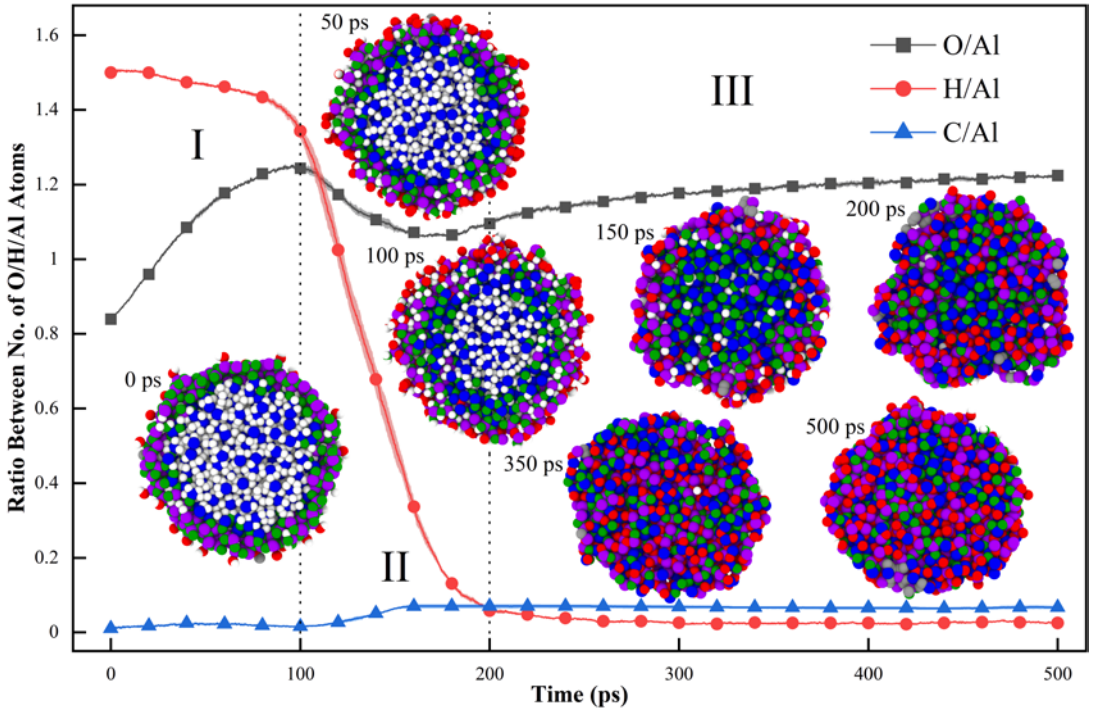

Fig. 4. Ratio between the numbers of O/H/C/Al atoms and snapshots of the central cross-sections of the AlH_3/Al_2O_3 core-shell nanoparticle during the overall oxidation process. The results after 500 ps are ignored due to the insignificant change.

The composition of the nanoparticle during the oxidation is also tracked as shown in Fig. 4. The number of Al atoms in the nanoparticle is constant throughout. At Stage I, the slow drop in H/Al is caused by the departure of HTPB molecules from the nanoparticle surface rather than the generation of any product. On the contrary, O/Al increases as the nanoparticle is adsorbing the ambient O_2

molecules. With the fast product release, both H/Al and O/Al decrease at Stage II. The moderate growth of C/Al results from the aforementioned decomposition of HTPB/HTPB intermediates on the nanoparticle. O/Al in the last 20 ps of Stage II has begun to rise because the product release is about to finish but the nanoparticle keeps adsorbing the ambient O_2 molecules. Stage III presents a smooth variation in both H/Al and O/Al, where the liberation of H atoms reaches its maximum and the nanoparticle is slowly and continuously oxidized. At the end of the simulation (1000 ps), O/Al is appropriately 1.25. It can be expected that as the reaction progresses, a fully oxidized amorphous Al_2O_3 could be achieved eventually.

The obtained reaction mechanisms in the present research is consistent with the simplified model that Al oxidation takes place after the dehydrogenation of AlH_3 from the experimental study of [4]. Additionally, the previously reported overlapping of AlH_3 dehydrogenation and Al oxidation [13] is observed in Fig. 4 (snapshots at 100 and 150 ps). Also, the results are generally in good accordance with the previous MD study [21], which divided the oxidation of AlH_3/Al_2O_3 core-shell nanoparticle into three stages, namely, oxygen adsorption, fast dehydrogenation, and Al oxidation. However, the oxygen adsorption period is longer, and the fast dehydrogenation stage is slightly delayed in the present study. The reason is that HTPB molecules covering the nanoparticle obstruct the adsorption of ambient O_2 molecules at the beginning of the reaction.

3.3. Mechanisms of HTPB oxidation

Figure 5 describes the time evolution of the number of key species related to HTPB reaction during the overall oxidation process and the major mechanisms of HTPB oxidation are studied. It is found that the oxidation of HTPB is initiated by its decomposition. At Stage I, as mentioned before, some HTPB molecules lose their terminal H or OH when leaving the nanoparticle surface. Hence, $C_{20}H_{31}O$ and $C_{20}H_{31}O_2$ first appear and the formation of $C_{20}H_{31}O$ is earlier than that of $C_{20}H_{31}O_2$, which means dehydroxylation occurs at a lower temperature than dehydrogenation of HTPB. Instead of the scission of carbon chain, the nanoparticle facilitates the HTPB initiation by dehydroxylation or

dehydrogenation. The production of $C_{20}H_{31}O_2$ continues to increase at Stage II but the contribution mainly comes from the dehydrogenation of HTPB by ambient O_2 molecules. Consequently, the number of HTPB reduces and the HO_2 generation grows. Meanwhile, the C-C bond at either end of HTPB or its intermediates is broken producing C_4H_6, C_4H_6O and C_4H_6OH. However, the reaction of HTPB does not progress much as Stage II is dominated by the fast product release of the nanoparticle. After about 300 ps at Stage III, the production of these C_4 species, especially C_4H_6 sees dramatic growth. It is observed that after the cleavage of terminal C_4 units, the scission of the remaining carbon chain still begins with its terminal C_4 parts, resulting in the significant production of C_4H_6. Therefore, C_4 species are the key intermediates during the oxidation of HTPB. This finding should also be applicable to HTPB with a longer carbon chain. At a later stage of the reaction, the number of C_4 species drops as they are further oxidized to finally form CO, CO_2 and H_2O. The increase in H_2 production after about 700 ps is triggered by the pyrolysis and dehydrogenation of hydrocarbons under high temperature.

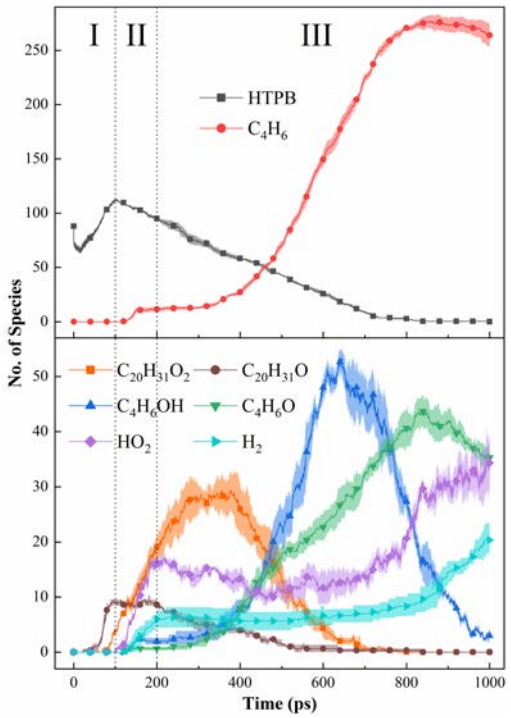

Fig. 5. Time evolution of the number of key species related to HTPB reaction during the overall oxidation process.

3.4. Discussion on the simplification of HTPB model

The solid HTPB in reality may have a relative molecular mass of several million terminated with a hydroxyl group at each end. A simplified HTPB model of $C_{20}H_{32}O_2$ is adopted in the present research because it is impractical to employ a realistic HTPB model together with the corresponding micron-size AlH_3/Al_2O_3 particle in ReaxFF MD simulations considering the current computational capability. This simplification leads to relatively excessive number of hydroxyl groups in the simulation system. As a result, in the real situation, the OH adsorption phenomenon of a HTPB molecule shown in Fig. 3d would be hardly found. Similarly, the dihydroxylation and dehydrogenation of HTPB described in Section 3.3 would be less evident. Nevertheless, the major decomposition products of HTPB obtained from the simulation including C_2H_4, C_4H_6 and C_5H_6 are in good agreement with experimental results [29]. Especially, C_4H_6 is identified as a dominant product in both simulation and experiment. Due to the simplified short chain HTPB model, the formation of cyclic intermediates as seen in the experiment is not remarkable here.

4. Conclusions

The fundamental oxidation mechanisms of AlH_3/HTPB solid fuel are investigated using ReaxFF MD simulations. The results show that the overall oxidation proceeds in three main stages: (I) preheating: the system temperature rises, HTPB sublimates, and the nanoparticle adsorbs the ambient O_2 molecules; (II) acceleration: the nanoparticle dominates the reaction accompanied by considerable temperature increase and product release; (III) oxidation: nanoparticle oxidation is stabilized and HTPB leads the reaction with a smooth increase in system temperature. The duration of Stage (I) is approximately the same as that of Stage (II) and Stage (III) would be much longer until the end of the reaction. The mechanisms of AlH_3 and HTPB are also separately studied to further understand their different roles and mutual interactions during the overall oxidation process. Regarding the oxidation of the AlH_3 nanoparticle, the reaction is delayed in the present research due to the initial coverage of the nanoparticle surface by HTPB molecules that obstructs the adsorption of ambient O_2 molecules,

while the mechanisms generally agree well with previous experimental and computational studies. Additionally, it is found that some of the HTPB/HTPB intermediates decompose on the nanoparticle surface and the decomposed products could be integrated with the nanoparticle. Major mechanisms of HTPB oxidation are also proposed. It is shown that the nanoparticle promotes the HTPB initiation by dehydroxylation or dehydrogenation and the latter occurs at a higher temperature. The continuous scission of carbon chain to form a large amount of C_4 species is the primary decomposition pathway of HTPB/HTPB intermediates. Finally, the C_4 species are further oxidized to produce CO, CO_2 and H_2O. The findings from the present research could potentially benefit the design of AlH_3/HTPB-based solid propellants. For example, AlH_3 could be coated with a HTPB layer before formulating into the propellant to preserve its high hydrogen capacity and prevent passivation during storage as it would not affect the combustion performance of AlH_3.

Acknowledgements

Funding from the UK Engineering and Physical Sciences Research Council under the project "UK Consortium on Mesoscale Engineering Sciences (UKCOMES)" (Grant No. EP/R029598/1), and from the National Natural Science Foundation of China (Grant No. 51706057) and Open Research Fund Program of Science and Technology of Aerospace Chemical Power Laboratory (Grant No. STACPL220181B02-2) is gratefully acknowledged. The first author is also grateful for the support of "Shuimu Tsinghua Scholar" program from Tsinghua University.

References

[1] J.F. Guery, I.S. Chang, T. Shimada, M. Glick, D. Boury, E. Robert, J. Napior, R. Wardle, C. Perut, M. Calabro, R. Glick, H. Habu, N. Sekino, G. Vigier, B. d'Andrea, Solid propulsion for space applications: An updated roadmap, Acta Astronaut. 66 (1-2) (2010) 201-219.

[2] S.C. Shark, T.L. Pourpoint, S.F. Son, S.D. Heister, Performance of dicyclopentadiene/H_2O_2-based hybrid rocket motors with metal hydride additives, J. Propul. Power 29 (5) (2013) 1122-1129.

[3] T. Bazyn, H. Krier, N. Glumac, N. Shankar, X. Wang, T.L. Jackson, Decomposition of aluminum hydride under solid rocket motor conditions, J. Propul. Power 23 (2) (2007) 457-464.

[4] N. Eisenreich, A. Kessler, A. Koleczko, V. Weiser, On the kinetics of AlH_3 decomposition and the subsequent Al oxidation, Int. J. Hydrogen Energy 39 (11) (2014) 6286-6294.

[5] I.M.K. Ismail, T. Hawkins, Kinetics of thermal decomposition of aluminium hydride: I-non-isothermal decomposition under vacuum and in inert atmosphere (argon), Thermochim. Acta 439 (1-2) (2005) 32-43.

[6] V. Weiser, N. Eisenreich, A. Koleczko, E. Roth, On the oxidation and combustion of AlH_3 a potential fuel for rocket propellants and gas generators, Propellants, Explos., Pyrotech. 32 (3) (2007) 213-221.

[7] J. Graetz, J.J. Reilly, Thermodynamics of the α, β and γ polymorphs of AlH_3, J. Alloys Compd. 424 (1-2) (2006) 262-265.

[8] L.T. DeLuca, L. Galfetti, F. Severini, L. Rossettini, L. Meda, G. Marra, B. D'Andrea, V. Weiser, M. Calabro, A.B. Vorozhtsov, A.A. Glazunov, G.J. Pavlovets, Physical and ballistic characterization of AlH_3-based space propellants, Aerosp. Sci. Technol. 11 (1) (2007) 18-25.

[9] T. Bazyn, R. Eyer, H. Krier, N. Glumac, Combustion characteristics of aluminum hydride at elevated pressure and temperature, J. Propul. Power 20 (3) (2004) 427-431.

[10] P.B. Kempa, V. Thome, M. Herrmann, Structure, chemical and physical behavior of aluminum hydride, Part. Part. Syst. Charact. 26 (3) (2009) 132-137.

[11] F. Maggi, G. Gariani, L. Galfetti, L.T. DeLuca, Theoretical analysis of hydrides in solid and hybrid rocket propulsion, Int. J. Hydrogen Energy 37 (2) (2012) 1760-1769.

[12] G. Young, G.A. Risha, T.L. Connell, R.A. Yetter, Combustion of HTPB based solid fuels containing metals and metal hydrides with nitrous oxide, Propellants, Explos., Pyrotech. 44 (6) (2019) 744-750.

[13] S.H. Chen, Y. Tang, H.S. Yu, L.R. Bao, W. Zhang, L.T. DeLuca, R.Q. Shen, Y.H. Ye, The rapid H_2 release from AlH_3 dehydrogenation forming porous layer in AlH_3/hydroxyl-terminated polybutadiene (HTPB) fuels during combustion, J. Hazard. Mater. 371 (2019) 53-61.

[14] Q. Mao, A.C.T. van Duin, K.H. Luo, Investigation of methane oxidation by palladium-based catalyst via ReaxFF Molecular Dynamics simulation, Proc. Combust. Inst. 36 (2017) 4339-4346.

[15] T.P. Senftle, S. Hong, M.M. Islam, S.B. Kylasa, Y. Zheng, Y.K. Shin, C. Junkermeier, R. Engel-Herbert, M.J. Janik, H.M. Aktulga, T. Verstraelen, A. Grama, A.C.T. van Duin, The ReaxFF reactive force-field: development, applications and future directions, npj Comput. Mater. 2 (2016) 15011.

[16] C. Ashraf, A.C.T. van Duin, Extension of the ReaxFF combustion force field toward syngas combustion and initial oxidation kinetics, J. Phys. Chem. A 121 (5) (2017) 1051-1068.

[17] M. Feng, X.Z. Jiang, K.H. Luo, A reactive molecular dynamics simulation study of methane oxidation assisted by platinum/graphene-based catalysts, Proc. Combust. Inst. 37 (2019) 5473-5480.

[18] M. Feng, X.Z. Jiang, Q. Mao, K.H. Luo, P. Hellier, Initiation mechanisms of enhanced pyrolysis and oxidation of JP-10 (exo-tetrahydrodicyclopentadiene) on functionalized graphene sheets: Insights from ReaxFF molecular dynamics simulations, Fuel 254 (2019) 115643.

[19] M. Feng, X.Z. Jiang, W. Zeng, K.H. Luo, P. Hellier, Ethanol oxidation with high water content: A reactive molecular dynamics simulation study, Fuel 235 (2019) 515-521.

[20] X.Z. Jiang, M. Feng, W. Zeng, K.H. Luo, Study of mechanisms for electric field effects on ethanol oxidation via reactive force field molecular dynamics, Proc. Combust. Inst. 37 (2019) 5525-5535.

[21] M. Feng, H. Li, Q. Mao, K.H. Luo, P. Hellier, Fundamental study on mechanisms of thermal decomposition and oxidation of aluminum hydride, J. Phys. Chem. C 123 (40) (2019) 24436-24445.

[22] S. Hong, A.C.T. van Duin, Atomistic-scale analysis of carbon coating and its effect on the oxidation of aluminum nanoparticles by ReaxFF-molecular dynamics simulations, J. Phys. Chem. C 120 (17) (2016) 9464-9474.

[23] J.G.O. Ojwang, R.A. van Santen, G.J. Kramer, A.C.T. van Duin, W.A. Goddard, Parametrization of a reactive force field for aluminum hydride, J. Chem. Phys. 131 (4) (2009) 044501.

[24] S. Plimpton, Fast parallel algorithms for short-range molecular dynamics, J. Comput. Phys. 117 (1) (1995) 1-19.

[25] A. Stukowski, Visualization and analysis of atomistic simulation data with OVITO-the Open Visualization Tool, Modell. Simul. Mater. Sci. Eng. 18 (1) (2010) 015012.

[26] Y. Li, R.K. Kalia, A. Nakano, P. Vashishta, Size effect on the oxidation of aluminum nanoparticle: Multimillion-atom reactive molecular dynamics simulations, J. Appl. Phys. 114 (13) (2013) 134312.

[27] S. Muto, K. Tatsumi, K. Ikeda, S. Orimo, Dehydriding process of α-AlH3 observed by transmission electron microscopy and electron energy-loss spectroscopy, J. Appl. Phys. 105 (12) (2009) 123514.

[28] A. Singh, S. Radhakrishnan, R. Vijayalakshmi, M.B. Talawar, A. Kumar, D. Kumar, Screening of polymer-plasticizer systems for propellant binder applications: an experimental and simulation approach, J. Energ. Mater. 37 (4) (2019) 365–377.

[29] K.K. Kuo, M.J. Chiaverini (Eds.), Fundamentals of Hybrid Rocket Combustion and Propulsion, American Institute of Aeronautics and Astronautics, Virginia, 2007, p. 610.

List of Figure Captions

Fig. 1. Illustration of key stages and potential energy profiles of relaxation and equilibration processes during the system construction: (a) relaxed core-shell AlH_3/Al_2O_3 structure; (b) energy minimized HTPB molecule; (c) equilibrated AlH_3/Al_2O_3-HTPB composite (orange circles show the typical nanoparticle exposed areas); (d) oxidation simulation system; (e) potential energy profiles of relaxation and equilibration processes. Atoms colouring scheme: core Al - blue; shell Al - purple; H - white; shell O - green; HTPB & molecular oxygen O - red; C - grey.

Fig. 2. Three main stages for the oxidation reaction characterised by the time evolution of (a) temperature and (b) number of key species. Stage I (0-100 ps): preheating; Stage II (100-200 ps): acceleration; Stage III (200 ps onward): moderate oxidation.

Fig. 3. Process of HTPB sublimation during Stage I of the oxidation reaction: (a) t = 20 ps; (b) t = 60 ps; (c) t = 100 ps; (d) an example of O of OH from one end of HTPB adhering on the nanoparticle surface Al atom with the carbon chain freely hanging in the air. Only the nanoparticle and HTPB molecules are shown for a clear visualization.

Fig. 4. Ratio between the numbers of O/H/C/Al atoms and snapshots of the central cross-sections of the AlH_3/Al_2O_3 core-shell nanoparticle during the overall oxidation process. The results after 500 ps are ignored due to the insignificant change.

Fig. 5. Time evolution of the number of key species related to HTPB reaction during the overall oxidation process.